The EMBO Journal Vol.17 No.17 pp.4943–4953, 1998

Clathrin coats at 21 Å resolution: a cellular assembly designed to recycle multiple membrane receptors

Corinne J.Smith[1], Nikolaus Grigorieff and Barbara M.F.Pearse

MRC Laboratory of Molecular Biology, Hills Road, Cambridge CB2 2QH, UK

[1]Corresponding author
e-mail: cs1@mrc-lmb.cam.ac.uk

We present a map at 21 Å resolution of clathrin assembled into cages with the endocytic adaptor complex, AP-2. The map was obtained by cryo-electron microscopy and single-particle reconstruction. It reveals details of the packing of entire clathrin molecules as they interact to form a cage with two nested polyhedral layers. The proximal domains of each triskelion leg depart from a cage vertex in a skewed orientation, forming a slightly twisted bundle with three other leg domains. Thus, each triskelion contributes to two connecting edges of the polyhedral cage. The clathrin heavy chains continue inwards under the vertices with local 3-fold symmetry, the terminal domains contributing to 'hook-like' features which form an intermediate network making possible contacts with the surface presented by the inner adaptor shell. A node of density projecting inwards from the vertex may correspond to the C-termini of clathrin heavy chains which form a protrusion on free triskelions at the vertex. The inter-subunit interactions visible in this map provide a structural basis for considering the assembly of clathrin coats on a membrane and show the contacts which will need to be disrupted during disassembly.

Keywords: 3D structure/AP-2 adaptor/clathrin/cryo-electron microscopy/single-particle analysis

Introduction

Clathrin forms the honeycomb lattice on the cytoplasmic surface of coated pits found both on the plasma membrane and at certain intracellular sites, e.g. the *trans*-Golgi network (TGN). In combination with the specific adaptor complexes (AP-2 at the plasma membrane and AP-1 on the TGN), clathrin participates in making a coat structure capable of deforming the membrane into an invaginated bud, in which selected recycling receptors bearing appropriate signals are generally concentrated. The buds are then pinched off to form transport vesicles which participate in endosome formation, depending on the targeting and fusion molecules carried by the vesicles. This mechanism is most obviously used at the plasma membrane in receptor-mediated endocytosis (Roth and Porter, 1964), to concentrate and deliver nutrients to the cell (e.g. in the human placenta). The process of constantly selecting and recycling receptors through coated pits and the endosome network allows cells to set up and remodel their peripheral membrane compartments, particularly in response to external factors (e.g. in nerve synapses; Heuser and Reese, 1973; Bailey *et al*., 1992; Maycox *et al*., 1992; Prior and Clague, 1997; Solomonia *et al*., 1997). Thus it has become increasingly evident that the cycle of budding transport vesicles with clathrin coats is a highly dynamic, exquisitely controlled process. It requires ATP for clathrin disassembly (via auxilin and hsc70; Schlossman *et al*., 1984; Ungewickell *et al*., 1995; Barouch *et al*., 1997) and GTP at numerous steps in the process, including functional coated pit formation involving rab5 (McLauchlan *et al*., 1997), and particularly the release of the coated vesicles by dynamin (for a recent review see Schmid, 1997).

So far the only available three-dimensional (3D) description of the clathrin coat (reassembled from purified clathrin and adaptors) is the map determined by cryo-electron microscopy by Vigers *et al*. (1986a,b), by averaging tilt series about the 6-fold axis of the hexagonal barrel type of clathrin cage. This map shows the overall shape of the cage and three nested shells of density of the coat, corresponding to the outer clathrin cage, the clathrin heavy-chain terminal domains and the inner adaptor layer, respectively. This map was obtained early in the development of cryo-electron microscopy of non-crystalline structures and techniques have now improved considerably. We present here a map at 21 Å resolution of clathrin assembled with the AP-2 adaptor complex into the hexagonal barrel cage arrangement. This higher resolution study reveals how the three-legged clathrin triskelion molecules (one centred at each vertex and composed of three 180 kDa heavy chains and three attendant light chains) interact via their proximal and distal leg portions to form the polyhedral outer cage, while the terminal domains of the heavy chains form an inner network which appears to make contact with the adaptor layer.

Results

Sample preparation and cryo-electron microscopy

Coats formed from an assembly of purified clathrin and AP-2 are shown in the electron micrograph of the frozen hydrated specimen in Figure 1b. Analysis by sodium dodecyl sulfate–polyacrylamide gel electrophoresis (SDS–PAGE) of the sample used for electron microscopy (Figure 1a) shows clathrin heavy chains and light chains, together with the 100 kDa α and β adaptin polypeptides and the 50 kDa μ subunits and 16 kDa σ subunits of the heterotetrameric adaptor AP-2 (in the region of one adaptor complex per triskelion). A diagram showing features of a clathrin triskelion is shown in Figure 1c for reference.

The electron micrograph illustrates the heterogeneity of the assembled coats. Although, to some extent, the size

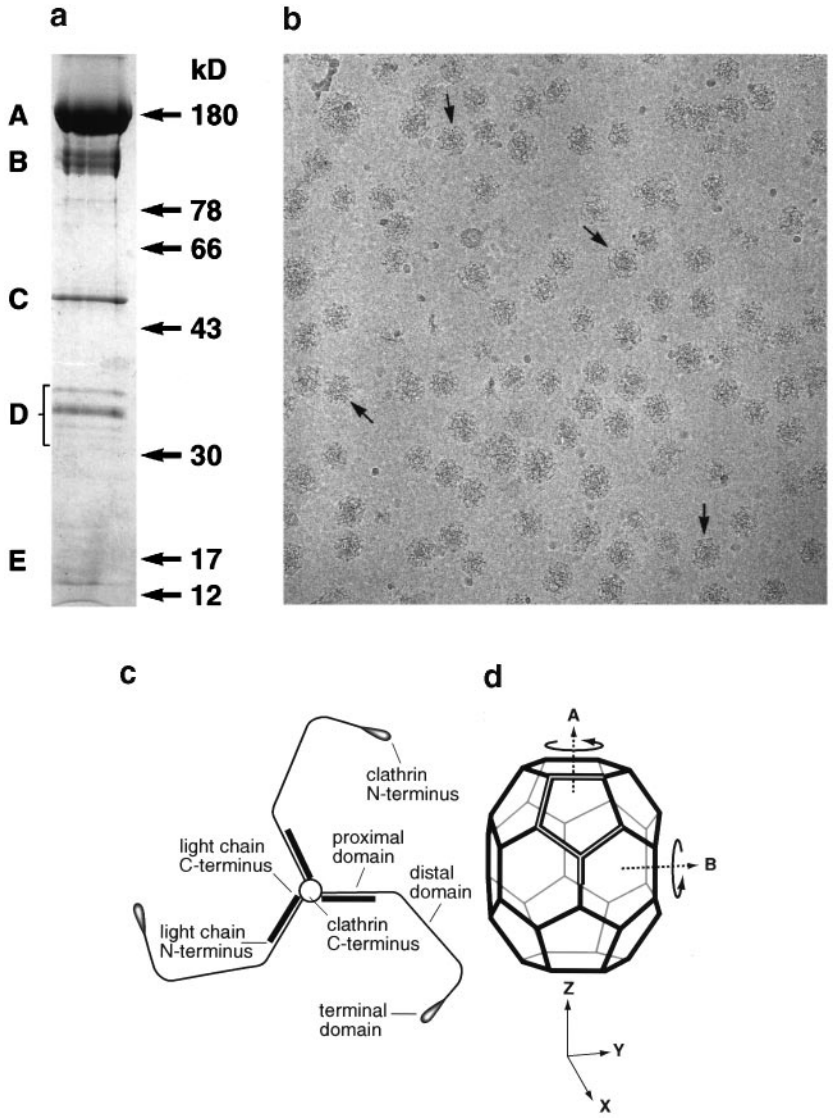

Fig. 1. (**a**) Composition of clathrin and AP-2 complex analysed by SDS–PAGE. Labelled bands correspond to clathrin heavy chain (A), α and β adaptins (B), μ subunit (C), the clathrin light chains (D) and the σ subunit (E). The mol. wts of the markers are shown on the right. (**b**) Typical image of assembled adaptor complexes in vitreous ice with potential hexagonal barrels indicated by the arrows. The width of the cages marked by arrows is ~70 nm. (**c**) Schematic diagram of clathrin triskelion. This is a simple representation of the position of the light chains. One alternative view suggests that the light chains perform a U-turn on the proximal leg such that the termini come together towards a vertex (Näthke *et al.*, 1992). (**d**) Diagram of a hexagonal barrel showing the location of the symmetry axes and an asymmetric unit of the barrel (white edges). The dashed arrow (A) marks the 6-fold symmetry axis and the arrow labelled (B) marks 2-fold symmetry axis. The *x*, *y* and *z* axes are defined such that they intersect at the centre of the barrel.

range of the cages can be controlled by the assembly conditions it is not possible to obtain a homogenous preparation of a single cage type. This is because many different cage arrangements are still possible even within a narrow size range, for example, the 'tennis ball' type is close in size to the 'hexagonal barrel' (Crowther *et al.*, 1976). With small cages there are fewer possible arrangements and, therefore, the smallest symmetrical cage type, the hexagonal barrel (shown in Figure 1d), is relatively common in a preparation of the appropriate size range. This cage type possesses 622 symmetry (Crowther *et al.*, 1976) and images of these in ice display an approximate centre of symmetry. Both this symmetry and the size of the barrels were used to select barrel-type particles by eye for further processing. The particle type was verified, during image processing, by comparing each image with the best-matching projection of the current best 3D reference map, during alignment (see Materials and methods).

Image processing

Initially, 1244 particles were selected from 100 micrographs. The structure determination was then performed in two stages (described in full in Materials and methods). First, the orientations of the particles were determined by comparison with the existing map (Vigers *et al.*, 1986b) using a projection-matching procedure (Harauz and Ottensmeyer, 1984; Penczek *et al.*, 1994). This was part of the SPIDER package of image processing software (Frank *et al.*, 1981, 1996). A map of ~40 Å resolution resulting from this procedure was then improved using a new program, FREALIGN (Grigorieff, 1998).

Altogether, 1158 'good' particles with phase residuals

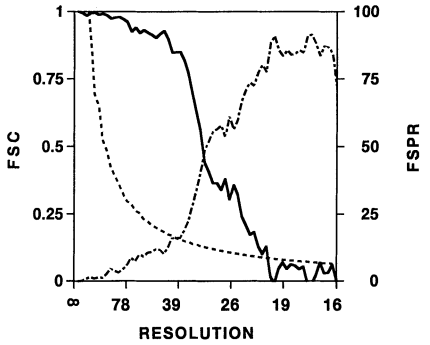

Fig. 2. Graph of Fourier shell correlation (FSC; unbroken line), critical Fourier shell correlation (CFSC; dashed line) and Fourier shell phase residuals (FSPR; dashed and dotted line) against resolution (in Å) calculated from two independent maps, each reconstructed from half the total number of particles.

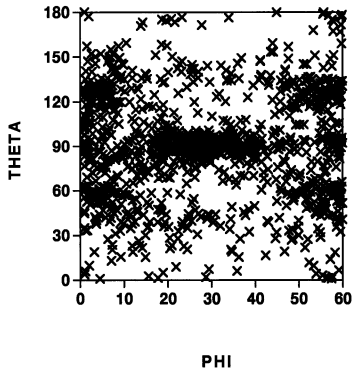

Fig. 3. Distribution of angles of the 1158 particles included in the final reconstruction of the clathrin assembly. Phi is the angle of rotation about the *z*-axis, around the 6-fold symmetry axis and theta is the angle of rotation about the new *y*-axis. There are preferred orientations around values of theta of 60, 90 and 120°.

below 82° to a resolution of 21 Å contributed to the final structure. The resolution of the map was estimated from a plot of the Fourier shell correlation (see Materials and methods) shown in Figure 2. Also shown in Figure 2 are the Fourier shell phase residual and a plot of values for the Fourier shell correlation estimated for pure noise (see Materials and methods) (Harauz and Van Heel, 1986; Van Heel, 1987). The Fourier shell correlation falls to 0.5 (the resolution criterion used in Böttcher *et al*., 1997) at a spacing of 32 Å. The Fourier shell correlation crosses the significance level at a spacing of 21 Å. The map shown here has therefore been filtered to a resolution of 21 Å.

Figure 3 shows the distribution of angles, theta and phi, for all the particles used in the reconstruction. Phi is the angle of rotation about the *z*-axis and theta is the angle of rotation about the new *y*-axis (Figure 1d). Figure 4 is viewed from the *x*-axis, with the *z*-axis vertical. Some anisotropy in the distribution of views of particles is revealed (Figure 3). There are clusters of points around the theta angles 60, 90 and 120° but values of phi at these angles were fairly evenly distributed. The anisotropy is likely to be due to barrels adopting preferred orientations in the thin layer of water formed just before freezing. The possibility that there was some bias in choosing particles cannot be ruled out as certain views are more easily recognized. The uneven distribution of angles does not cause any significant anisotropy in the resolution of the map, as indicated by the point spread function (not shown) calculated for the map (Grigorieff, 1998).

Based on the previous studies carried out by Vigers *et al*. (1986a,b), 622 point group symmetry was imposed on the map. The location of the 6- and 2-fold symmetry axes is illustrated in Figure 1d. When the whole map is symmetry averaged, 12 asymmetric units, each consisting of a 60° segment, half the height of the barrel, become computationally identical. Each asymmetric unit contains three triskelions which are quasi-equivalently related because of the geometry of the hexagonal barrel, but for which symmetry was not imposed. Considering the edges of the cage, there are 4.5 computationally independent edges, highlighted in Figure 1d. These form four out of five edges of each pentagonal face, and can be said to meet at two neighbouring independent vertices of the equatorial hexagonal faces. The degree to which local symmetry is maintained at the pentagonal faces and at the independent vertices of the equatorial hexagons therefore indicates the reliability of any features seen in the map.

Overall description of the map

A surface representation of the whole complex is shown as a stereo pair (Figure 4). There are a number of striking differences between this new map and the map obtained by Vigers *et al*. (1986b) due to a substantial improvement in the resolution. In the clathrin cage, details of individual triskelion legs are clearly seen for the first time. Also evident is a distinct skew to the structure at each vertex, showing the handedness observed in the previous structure. A schematic diagram (Figure 1c) of the clathrin triskelion is shown for reference.

Each edge of the hexagonal barrel consists of four segments of leg, each part of four different triskelions. The proximal domains form an anti-parallel pair on the top of an edge and the distal domains make an anti-parallel pair beneath them. This means that the edges possess local 2-fold symmetry around an axis perpendicular to the surface of the shell. All four legs make close contact with each other, particularly towards the centre of the edge. The high contour level of Figure 5 allows these areas of close contact to be seen more easily. The position of a hub at the centre of each vertex, together with the skew present at the hub seem to introduce a slight twist to each edge. This twist can be also observed in Figure 5.

The pentagonal faces are of interest since four out of five edges on each face are computationally independent, yet 5-fold symmetry of all the features observed within each face is clearly seen (Figure 6). The noise present in the structure can be assessed by comparison of the 'hook-like' features present within the edges of the pentagon.

At the vertex the upper and lower layers contributed by different triskelion legs are more separated as the lower layer consists, at this point, of terminal domains beginning to protrude into the centre of the cage. Interestingly, Figure 7 reveals a node of density at the hub directly beneath the top layer of legs at the vertex which is likely to include the C-terminus of the clathrin heavy chain.

The path of a triskelion leg

The following section contains our interpretation of the density in terms of the path of one leg of a triskelion,

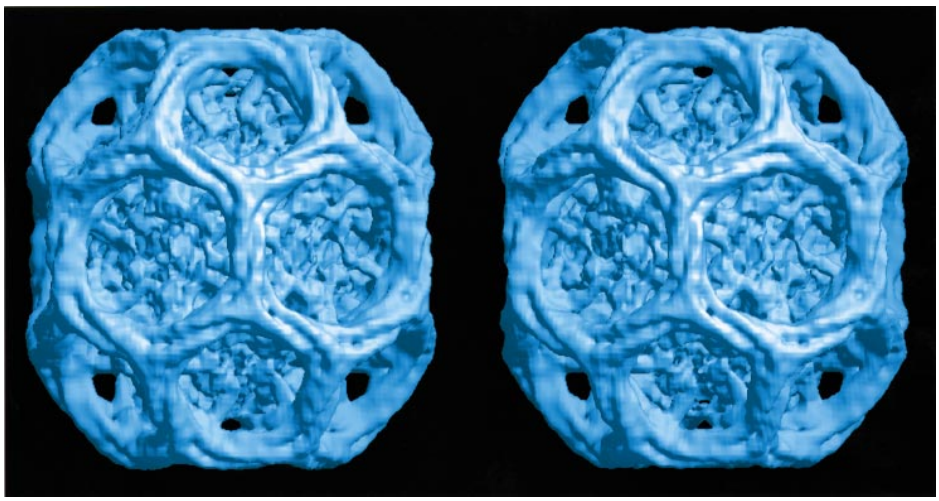

Fig. 4. Surface represention of the refined map of the clathrin–AP-2 complex shown as a stereo pair. The map was filtered to a resolution of 21 Å. We estimate the distance between each vertex to be 185 ± 10 Å while the width of whole assembly (measured between the widest points) is ~700 ± 10 Å.

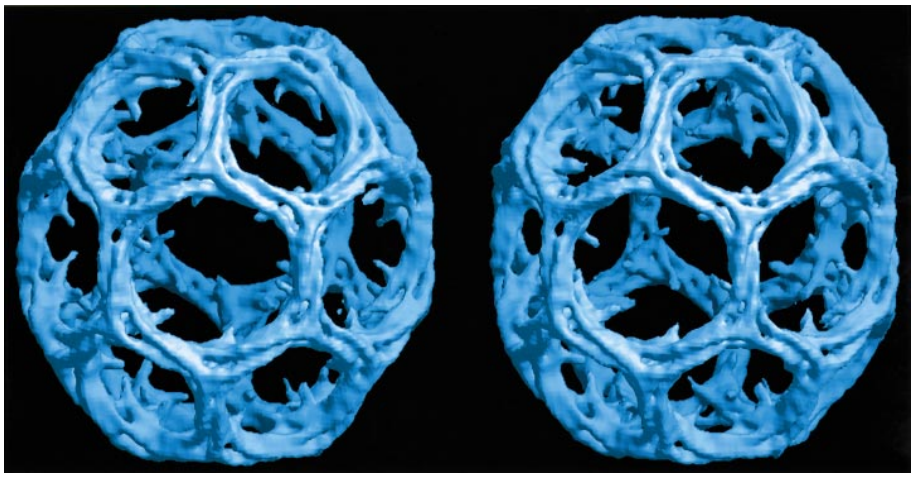

Fig. 5. A representation of the clathrin-adaptor map at a high contour level with an ellipsoid including the inner core of adaptors removed in order to show the path followed by the triskelion legs (shown as a stereo pair). At this contour level the terminal domains are truncated.

starting at a vertex and continuing through to the adaptor layer. Figure 5 shows the whole cage (as a stereo pair) at a high contour level with the central core removed. At this contour level, and with the centre removed, regions beneath the vertex including the terminal domains are truncated.

The portrayal of the map given in Figure 7 shows shells of density of 7.8 Å thickness peeled off in sequence, like onion layers, from the whole top half of the map. By examination of Figures 5 and 7 it is possible to trace the path of a leg from the hub, along an edge veering past the next vertex, then along under a second edge towards a further vertex, and then turning inwards under that vertex. In Figure 7 the first four shells (on rows 1 and 2) show two strands lying against each other. It is clear from this that at least the top two strands (the proximal domains) lie side-by-side without crossing over. In shells five and six it might be thought that the distal strands cross over. However, the size and relatively smooth appearance of the edges of the polyhedron suggest that this is not the case, and that the observed density pattern is due to the twist present in the edges. Hence it appears to us that the legs lie against each other, curving round in the same direction, and do not cross until the transition from distal domain to terminal domain in the region beneath the vertex. Packing side-by-side, rather than crossing over, would serve to maximize the area of contact between the legs.

As the distal domain travels towards, and then becomes, the terminal domain it seems most likely that it continues straight past the vertex (without bending sharply), moving inwards at the same time, and crossing the other terminal domains which meet at that point. The terminal domains continue inward towards the adaptor complex, forming 'hook-like' structures and a network with other legs. Density continuous with the terminal domains then appears to make contact (Figure 8) with the surface of the adaptor layer. The noise level at this resolution is such that not all symmetry-related domains make obvious contact (Figure 8) with the adaptor surface.

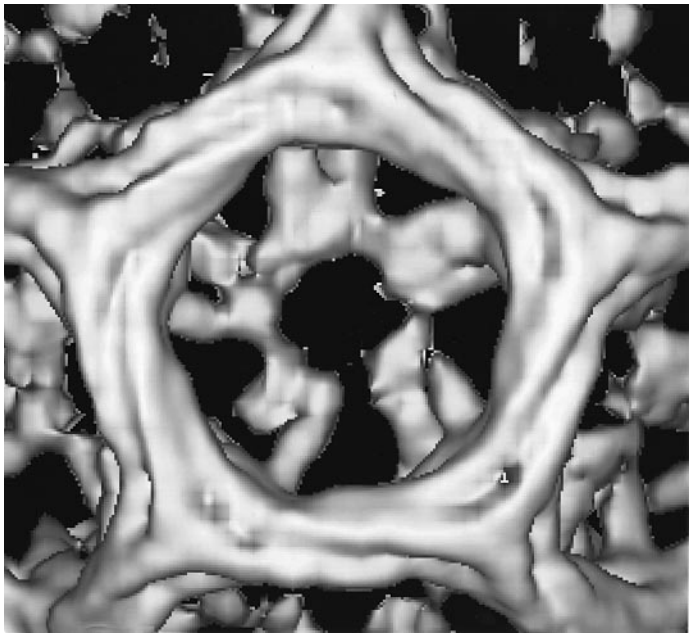

Fig. 6. Close-up of the outside of a pentagonal face showing terminal domains forming an inner network inside the face. Since four out of five edges of the pentagon are computationally independent, the degree to which the local 5-fold symmetry is maintained is a good indication of the reliability of the map.

We attribute the density which emerges from the third vertex and bends round to form a 'hook' to the clathrin terminal domain since this is consistent with the interpretation made by Vigers *et al*. (1986a,b) but the precise end-point of the terminal domains is not yet resolved. Measurement of the length of the density we attribute to the clathrin leg, to the point where the terminal domains appear to meet results in an estimate of ~420 Å, which is close to the previously published estimates for stained triskelions, 433 ± 43 Å (Crowther and Pearse, 1981) and 450 ± 23 Å (Ungewickell and Branton, 1981). Further density of length ~50 Å continues towards the main adaptor shell and at least a part of this may also be due to the terminal domains.

Nature of terminal domains and their relationship to the adaptor shell

Beneath each vertex three distal domains curve inwards towards the centre with local 3-fold symmetry (Figures 5 and 7) continuing as the clathrin terminal domains. In Figure 7 (rows 3 and 4) these three fingers of density spread outwards as they move through the layers and appear to link up to make a network mimicking the geometry of the barrel (row 5). This network can also be seen in Figure 4 inside the edges of the outer cage.

Figure 9 shows in close-up a representative view of a vertex, viewed from inside the cage with the central adaptor core removed. Density traced along a terminal domain ends in a kink which folds back on itself to form a 'hook' at the end of the leg and density continuous with this structure then appears to make contact with the main adaptor shell. The precise appearance of the hooks is not fully defined at this resolution. The vertex chosen for Figure 9 has independent edges leading from it and the noise level can be judged from the fact that two out of the three hooks are connected by density while the third is set apart. Figure 6 shows a different view of the 'hook-like' features. Viewed from the outside of the cage, they can be seen within the edges of the pentagon.

As was observed by Vigers *et al*. (1986b), the adaptors form a core in the centre of the clathrin cage. The density of the adaptor complex is almost continuous at this resolution, implying that the complexes are tightly packed. The central hole is less evident here than in the previous structure but there is a suggestion of a cavity in the interior (Figure 8).

Discussion

We present a 3D map of the hexagonal barrel form of the clathrin coat which reveals for the first time the arrangement of entire clathrin molecules in their functional location.

3D packing of the triskelions

The most striking feature of the complete coat viewed from the cytoplasmic aspect in this map is the 3D packing arrangement of the clathrin triskelion legs since details of individual legs can now be distinguished. The gross geometry of the clathrin outer cage structure corresponds to earlier models (Crowther and Pearse, 1981; Vigers *et al*., 1986a) and shows the characteristic skewed pattern of hexagonal and pentagonal 'windows'. As predicted previously, from the original study of clathrin assemblies by electron microscopy of specimens in negative stain, each triskelion centred at a vertex projects a proximal leg towards each of the three neighbouring vertices in a slightly skewed direction. Each triskelion leg then kinks such that the distal portion contributes to a further edge of a window. The way in which this is achieved is revealed in Figure 7 by examining thin shells of the structure, peeled off layer by layer, following individual triskelion

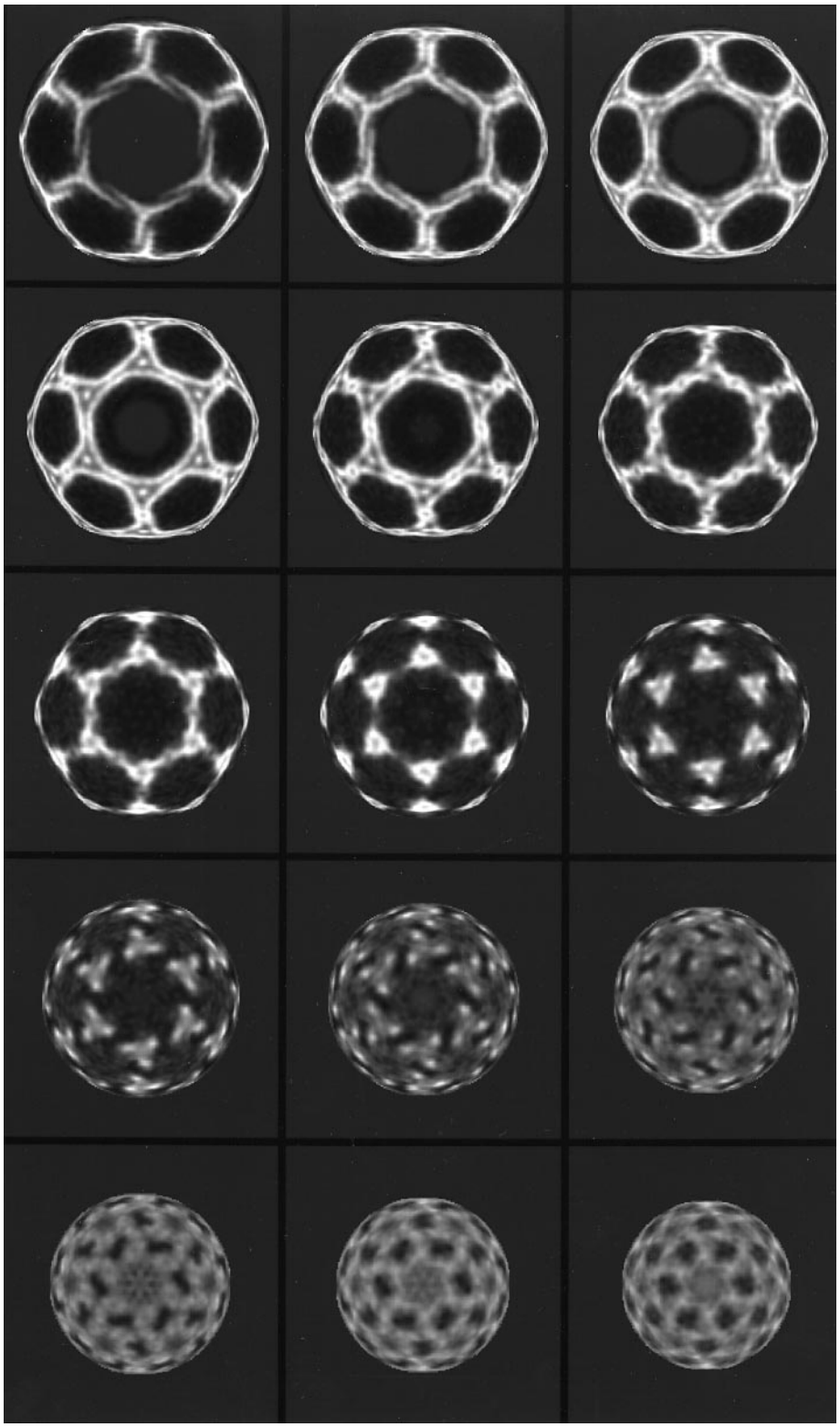

Fig. 7. The map shown in Figure 4 is represented as a sequence of ellipsoid half-shells of thickness 7.8 Å of decreasing radius. The top left image represents the largest shell and the size decreases sequentially from left to right moving down the figure. The images of the shells are also numbered in this order. Only the top half of the map is shown (around the 6-fold symmetry axis) with the outermost layer (at a radius of ~327 Å) at the top left hand corner. The inner shells from an approximate radius of 220 Å are not shown. The top two rows (shells 1–6) show detail of the packing of the proximal and distal domains while rows three and four (shells 7–12) show the local 3-fold symmetry of the heavy chain terminal domains which project inward to form an inner ring of density (row five, shells 13–15).

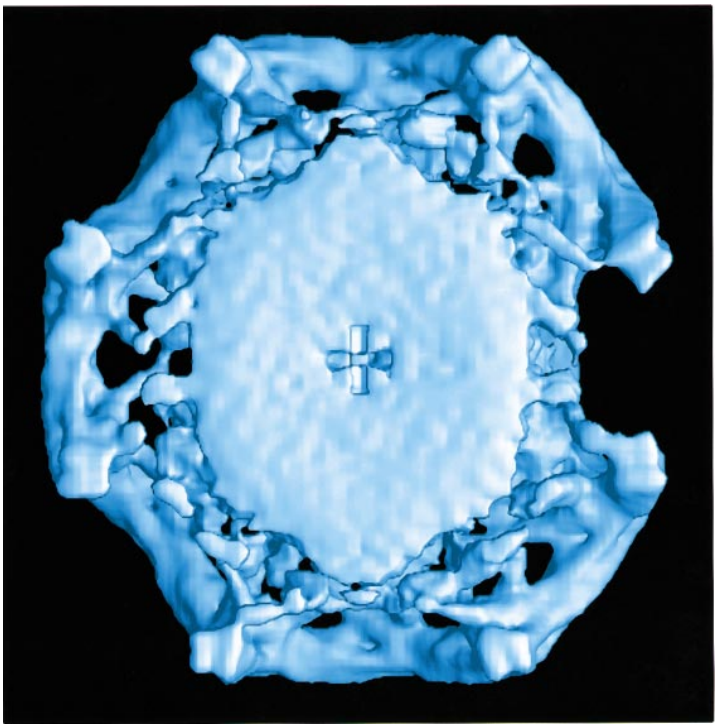

Fig. 8. Clathrin-adaptor map sliced in half at an angle of phi of 45° and viewed perpendicular to the sliced face with the *z*-axis vertical. This shows possible areas of contact between the adaptor shell and the clathrin legs.

legs as they contribute to the scaffolding at different levels, through the cage and into the interior. From this we deduce that the proximal and distal domains of different legs lie side-by-side in a slightly twisted bundle, with each leg curling round in the same direction (e.g. as seen in some views of free triskelions). As each distal leg portion approaches its far vertex it curves into the interior of the cage and finally the terminal domains make a second layer of material around the shell of adaptors. Overall, the three shells of density described in the first clathrin coat structure are seen here but the arrangement of the legs is resolved in much greater detail. In particular, the middle shell in the previous structure containing the terminal domains has resolved into a fine 'net' spreading over the surface of the adaptors with the ends joined in a roughly hexagonal or pentagonal pattern.

Location of known features of the clathrin triskelion hub in the map

Each triskelion hub is centred at a vertex of the cage structure. Exploration of the domain structure of purified triskelions by proteolysis, antibody binding and reconstitution of expressed fragments of the heavy and light chains, combined with mutational studies, has led to the proposal of quite detailed models of how the hub region may be constructed from three C-terminal regions of the heavy chain with the addition of three attendant light chains (Ungewickell, 1983; Näthke *et al*., 1992; Kirchhausen and Toyoda, 1993; Liu *et al*., 1995; Pishvaee *et al*., 1997). The clathrin light chains provide potential targets for modulation of the angles at the hub and also can play a role in controlling interactions between the clathrin leg regions during cage formation (Ungewickell and Ungewickell, 1991; Liu *et al*., 1995; Ybe *et al*., 1998).

At the vertices in the map there is a central region of density on the inner surface which may correlate with the ends of the clathrin heavy chains encompassing the globular C-terminal regions of sequence (residues 1590–1675 of the bovine sequence), as suggested by Näthke *et al*. (1992). This density projects inwards at the vertex through shells three to five in Figure 7. Since each shell is ~8 Å thick this suggests that the density spans a distance of ~25 Å, remaining within the thickness of the outer polyhedral cage but not extending into the shells occupied by the terminal domains. This contrasts with some proposed models in which the globular C-terminal regions protrude outwards from the trimer hub. This idea led to speculation that their interaction with cytoplasmic determinants might influence hub angles, perhaps via interaction with the light chains (Näthke *et al*., 1992; Liu *et al*., 1995; Pishvaee *et al*., 1997). Examination of Figure 5 suggests that the structure surrounding the node of density is fairly open and may be accessible to other proteins while at the same time it may contact the proximal and distal domains. However, the residues at the extreme C-terminus vary considerably between species (Blackbourn and Jackson, 1996) and analysis of a C-terminal mutant of yeast heavy chain has demonstrated that this globular protusion plays no essential role in triskelia assembly or clathrin function (Lemmon *et al*., 1991). The next portion of the sequence includes the predicted trimerization domain within residues 1490–1587 (of the yeast sequence) and within this is a possible α-helical segment (residues 1522–1572) (numbering from Pishvaee *et al*., 1997).

At the resolution of our map, it is not possible to identify the light chains, but these bind in the 'vertex-to-kink' region along the proximal leg. Light-chain binding

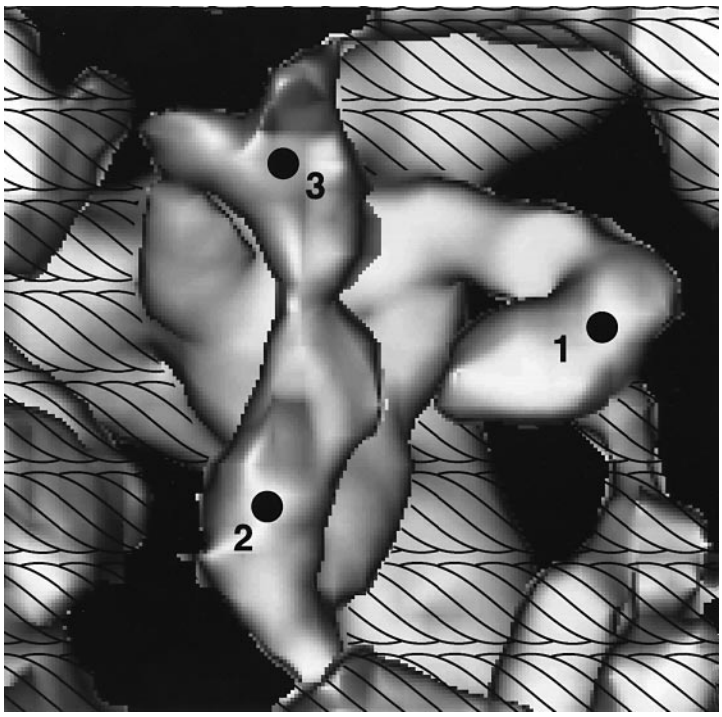

Fig. 9. Close-up of a vertex viewed from inside the clathrin cage to show clathrin terminal domains. An ellipsoid slightly larger than the adaptor shell was cut out of the map. The density emerges from the vertex with local 3-fold symmetry and curls round to form 'hook-like' features (labelled 1, 2 and 3). The differences in the shapes of the hooks indicate the level of noise. The view is slightly tilted away from the 3-fold axis to show the hook shape (1) and the rest of the map is shaded for clarity.

sites are thought to span residues 1213–1313, 1438–1481 and 1513–1522 (Pishvaee *et al*., 1997). The first kink in the leg (~18 nm from the vertex) is thought to occur after residue 1074 in the sequence. Clathrin triskelion fragments (residues 1074–1675) have been expressed in *Escherichia coli* and trimerized, with added attendant light chains, to form hub-like structures corresponding to the central hubs of complete triskelions. These reconstituted hubs will assemble under suitable conditions into rather irregular, flat, net-like structures rather than cages, with features resembling the full clathrin lattice. In addition, the hubs have been induced to crystallize (Liu *et al*., 1995). Contacts visible in the map between the distal leg portions and the anti-parallel proximal leg domains show how the triskelion legs bundle together to form a polyhedral cage. The terminal domains, constituting the N-terminal third of the heavy chains could also play a role in self-assembly of cages by triskelions. It therefore seems that the various interactions made by proximal, distal and terminal domains could all contribute to produce regular, curved cages rather than flat lattices.

Clearly, further improvement in resolution of the electron micrograph maps, in conjunction with X-ray crystallographic studies of clathrin domains, is required to relate the clathrin sequence to its structure in any more detail.

Clathrin terminal domains

In our map we attribute the density which progresses inwards from the vertex to the terminal domains of the clathrin triskelion (Vigers *et al*., 1986a,b). However, the precise point where the terminal domains end and density due to adaptors begins is not yet resolved. The difference maps produced by Vigers *et al*. (1986b) suggest that the terminal domains continue to the place where they appear to meet up and 'fingers' of density from the adaptors point towards the terminal domains. In our map the point where the terminal domains appear to meet is resolved into 'hook-like' features (Figure 9) which have 3-fold symmetry. These 'hooks' could account for the more globular appearance of the terminal domains in micrographs of single triskelions (e.g. Kirchhausen *et al*., 1986). The density from these continues towards the surface of the adaptor shell.

An earlier study, using deep-etch microscopy, showed AP-2 molecules bound to free triskelions on their terminal domains (Heuser and Keen, 1988). Some of the density seen amongst the terminal domains may be contributed by the adaptors as biochemical studies show that clathrin interacts with the hinge region of the β-adaptin subunit (Ahle and Ungewickell, 1989; Galluser and Kirchhausen, 1993). However, some contribution from other regions of the adaptor, e.g. from the α-adaptin subunit cannot be excluded at this stage.

Interestingly, a whole group of proteins, including β-adaptins, has been identified which bind to clathrin terminal domains depending on similar amino acid sequence motifs (Dell'Angelica *et al*., 1998). β-arrestin was first shown to bind to the clathrin terminal domains dependent on such a motif (Goodman *et al*., 1997). β-arrestin performs an adaptor-like function in the internalization of G-protein receptors whereas AP-2 is typically involved in the uptake of nutrients by recycling receptors in plasma membrane coated pits. Other members of the group make coated pits on the other membranes.

Coat assembly on a membrane

In the hexagonal barrel structure shown here the adaptor layer is very tightly packed and there is no room for a vesicle in the less dense central cavity. However, the coat thickness of isolated coated vesicles has been shown to be constant irrespective of vesicle size and consistently shows the three characteristic shells of density (Vigers *et al*., 1986b) which correspond to the outer clathrin cage, the terminal domains and the adaptor shell observed in coats assembled from purified constituents.

In the cell, clathrin assembly occurs on adaptor complexes recruited from the cytoplasm to a particular membrane where they in turn bind specified membrane receptors. How this is achieved on the appropriate membrane is still not understood, although an increasing number of factors are becoming implicated. These include GTP-binding proteins which are found in abundance in coated pits (see review by Schmid, 1997). One example is Rab5, thought to control vesicle fusion (Novick and Zerial, 1997) but also, apparently, playing a role in functional coated-pit formation (McLauchlan *et al*., 1997).

The assembly of the clathrin cage is probably best thought of as starting at the membrane. Adaptors, with associated receptors, recruit clathrin terminal domains, bridging between them, and thus nucleating assembly. The contacts between triskelion leg domains then result in the formation of the polyhedral structure. Other adaptors and receptors could then join on to the network of terminal domains. This dynamic assembly could be modulated until a completed coated pit is formed.

Disassembly of the clathrin cage, after a coated vesicle has been pinched off, requires the action of auxilin and hsc70, together with ATP. The structural changes required to achieve disassembly are not yet understood. The orderly 3D packing arrangement of the clathrin triskelions now revealed shows in more detail the interactions which must be undone to release the triskelions from the coat. Hence factors involved in disassembly must simultaneously disrupt triskelion contacts on the polyhedral edges and those regions of the terminal domains which are in contact with the adaptors. At the resolution achieved in this map it should be possible to visualize these and other clathrin-binding proteins in place, on their natural substrate.

Materials and methods

Protein purification

Six to twelve fresh pig brains were homogenized in HKM buffer (50 mM HEPES, 250 mM K acetate, 10 mM Mg Ac_2 0.02% NaN_3 0.2 mM phenylmethyl sulphonyl fluoride, adjusted to pH 7.0 with KOH) and spun at 5000 *g* for 20 min. The resulting supernatant was centrifuged at 96 000 *g* for 45 min. Coated vesicles were then obtained from the pellet following the method of Campbell *et al.* (1984). Coat proteins were obtained from the coated vesicles essentially following the method of Pearse and Robinson (1984) with the difference that the adaptor peak fraction from the gel filtration column was diluted 2-fold before loading onto the hydroxylapatite column. Auxilin was eluted first from the hydroxylapatite column as decribed by Barouch *et al*. (1994) and the column was subsequently re-equilibrated and the adaptors eluted as described by Pearse and Robinson (1984).

Purified clathrin and AP-2 adaptor proteins were assembled into coats as described by Vigers *et al.* (1986b). Coats were pelleted by centrifugation for 15 min at 82 000 *g*. A sample of the frozen mixture was analysed by SDS–PAGE (Figure 1a).

Freezing

The appropriate concentration for freezing of hexagonal barrels was estimated by electron microscopy of samples stained with 2% uranyl acetate. Three hundred mesh copper grids (Agar) were coated with a holey carbon film and glow discharged for 1 min in the presence of amylamine. Three microlitres of sample was applied to the carbon side of the grid and the grid was blotted from the non-carbon side with one layer of Whatman grade 1 filter paper, plunged into liquid ethane slurry and stored in liquid nitrogen (Dubochet *et al*., 1988; Toyoshima, 1989).

Cryo-electron microscopy

The frozen samples were viewed using a Philips EM420 microscope, operating at 120 kV, with a Gatan cryo-holder. Images were obtained under low dose conditions (electron dose ~10 e/Å^2) at 36 000 nominal magnification. Three defocus values were used: 2, 2.5 and 3 μm. All the micrographs for a particular defocus were obtained on one day. Every effort was made to ensure that the conditions under which images were obtained were the same for each session. Small variations in the magnification were kept to a minimum by keeping the objective lens current and specimen height constant. Because of this, no attempt was made to correct for any change in magnification of the particles. The ice thickness was estimated using its density in the image (Szilágyi and Berriman, 1994) and only cages in ice judged to be of thickness 900 Å or above were included.

Image reconstruction

Micrographs were scanned with a Zeiss-SCAI scanner using a step size of 28 μm which gave a pixel size corresponding to 7.8 Å on the sample. Scanned micrographs were viewed using Ximdisp which is part of the MRC image processing package (Crowther *et al*., 1996) and WEB, which is part of the SPIDER software package (Frank *et al*., 1981, 1996).

All image processing was performed within the SPIDER software package with the exception of the use of FREALIGN (Grigorieff, 1998), which was written to be used within SPIDER.

Hexagonal barrels were identified by eye, windowed out in 128 pixel squares and normalized to a standard deviation of 1. Typically, 5–30 suitable cages per micrograph were found. The normalized particles were then roughly centred using an average of the particles.

In view of the availability of an existing map of clathrin and adaptors, projection-matching (Harauz and Ottensmeyer, 1984; Penczek *et al*., 1994) was used to find the orientations of the particles. Initially the reference structure was derived from the map obtained by Vigers *et al.* (1986b) of clathrin assembled with mixed adaptor proteins.

For the projection-matching procedure the reference was projected in 869 projections to cover all orientations evenly at 2° intervals. In view of the 6-fold symmetry about the *z*-axis, only projections with values of phi between 0 and 59.9° were produced. For each particle, the best matching projection was found and used as a reference for re-centering.

After a second cycle of projection-matching a 3D reconstruction was calculated using R-weighted back projection (Radermacher, 1988; Penczek *et al*., 1992), including only those particles with phase residuals below 90° to 45 Å (104° corresponded to random noise images). Six-two-two symmetry was applied to the reconstruction. The resolution of the reconstruction was estimated at 45 Å by Fourier shell correlation between the 6-fold averaged map and its 2-fold symmetry-related map, before the 2-fold symmetry was imposed. The symmetrized reconstruction was then filtered to a resolution of 45 Å and used as a reference for the next alignment cycle, giving an improved resolution of 40 Å. In total 498 particles were included in this starting map; 192 from the 2 μm data set, 157 from the 2.5 μm data set and 149 from the 3 μm set.

No further iteration of this process was carried out—instead the map was refined using a new program, FREALIGN (Grigorieff, 1998). FREALIGN refines the orientations and centres of particles, corrects for the contrast transfer function (CTF) in an image and calculates a 3D reconstruction. In this case, the program was adapted to apply the 622 symmetry possessed by the hexagonal barrel. Initially all the particles were treated identically, with no allowance for the variation in defocus. For the refinement procedure using FREALIGN, however, more accurate defocus values were obtained by examining the Thon rings (Thon, 1966) in a Fourier transformed image. Particles entered the reconstruction with a resolution-dependent weighting function, similar to a temperature factor (Grigorieff, 1998). Particles with a phase residual against the reference of $>82°$ were excluded since it was at this phase residual threshold that the best resolution was obtained. The resolution of the final map was estimated from the Fourier shell correlation calculated between two structures determined independently from two half sets of the data. This was compared with the 3 σ significance threshold function [critical Fourier shell correlation (CFSC)] estimated for pure noise (Harauz and Van Heel, 1986) (Figure 3). The threshold function was

multiplied by $\alpha 12 = 3.46$ to account for the 12-fold redundancy of the 622 point group symmetry.

At all times during the refinement a test to distinguish between mirror images of particles was applied to ensure that the hand of all the particles was consistently determined. Although the absolute hand of individual triskelions was found by Kirchhausen *et al*. (1986) this is not known for the clathrin cage structure and we have not attempted to determine it here. All these features of the program, FREALIGN, are fully described in Grigorieff (1998).

Display of maps

Surface representations of the map were obtained either using Surf and Light (Vigers, 1986) or from within Web (Frank *et al*., 1996), and displayed using either Ximdisp (Crowther *et al*., 1996) or Web. All surface representations are displayed at a contour level of twice the standard deviation of the density except Figure 5 which is displayed at three times the standard deviation of the density. The map was displayed as ellipsoid shells using a program supplied by R.A.Crowther. All measurements in angstroms are calculated assuming a magnification of $\times$36 000.

Acknowledgements

We would like to thank P.N.T.Unwin for generous support and for instruction on cryo-electron microscopy techniques and R.A.Crowther for invaluable advice and many useful comments on this manuscript. We are grateful to L.Zhang for her continuing help and expertise.

References

Ahle,S. and Ungewickell,E. (1989) Identification of a clathrin binding subunit in the HA2 adapter protein complex. *J. Biol. Chem.*, **264**, 20089–20093.

Bailey,C.H., Chen,M., Keller,F. and Kandel,E.R. (1992) Serotonin-mediated endocytosis of APCAM – an early step of learning-related synaptic growth in aplysia. *Science*, **256**, 645–649.

Barouch,W., Prasad,K., Greene,L.E. and Eisenberg,E. (1994) ATPase activity associated with the uncoating of clathrin baskets by hsp70. *J. Biol. Chem.*, **269**, 28563–28568.

Barouch,W., Prasad,K., Greene,L. and Eisenberg,E. (1997) Auxilin-induced interaction of the molecular chaperone Hsc70 with clathrin baskets. *Biochemistry*, **36**, 4303–4308.

Blackbourn,H.D. and Jackson,A.P. (1996) Plant clathrin heavy chain—sequence analysis and restricted localization in growing pollen tubes. *J. Cell Sci.*, **109**, 777–786.

Böttcher,B., Wynne,S.A. and Crowther,R.A. (1997) Determination of the fold of the core protein of hepatitis B virus by electron microscopy. *Nature*, **386**, 88–91.

Campbell C., Squicciarini,J., Shia,M., Pilch,P.F. and Fine,R.E. (1984) Identification of a protein kinase as an intrinsic component of rat liver coated vesicles. *Biochemistry*, **23**, 4420–4426.

Crowther,R.A. and Pearse,B.M.F. (1981) Assembly and packing of clathrin into coats. *J. Cell Biol.*, **91**, 790–797.

Crowther,R.A., Finch,J.T. and Pearse,B.M.F. (1976) On the structure of coated vesicles. *J. Mol. Biol.*, **103**, 785–798.

Crowther,R.A., Henderson,R. and Smith,J.M. (1996) MRC image processing programs. *J. Struct. Biol.*, **116**, 9–16.

Dell'Angelica,E.C., Klumperman,J., Stoorvogel,W. and Bonifacino,J.S. (1998) Association of the AP-3 adaptor complex with clathrin. *Science*, **280**, 431–434.

Dubochet,J., Adrian,M., Chang,J.-J., Homo,J.-C., Lepault,J., McDowall,A.W. and Schultz,P. (1988) Cryo-electron microscopy of vitrified specimens. *Quart. Rev. Biophys.*, **21**, 129–228.

Frank,J., Shimkin,B. and Dowse,H. (1981) SPIDER – a modular software system for electron image processing. *Ultramicroscopy*, **6**, 343–358.

Frank,J., Radermacher,M., Penczek,P., Zhu,J., Li,Y., Ladjadj,M. and Leith,A. (1996) SPIDER and WEB: processing and visualisation of images in 3D electron microscopy and related fields. *J. Struct. Biol.*, **116**, 190–199.

Galluser,A. and Kirchhausen,T. (1993) The $\beta 1$ and $\beta 2$ subunits of the AP complexes are the clathrin coat assembly components. *EMBO J.*, **12**, 5237–5244.

Goodman,O.B., Krupnick,J.G., Gurevich,V.V., Benovie,J.L. and Keen,J.H. (1997) Arrestin/clathrin interactions—Localization of the arrestin binding locus to the clathrin terminal domain. *J. Biol. Chem.*, **272**, 15017–15022.

Grigorieff,N. (1998) Three-dimensional structure of bovine NADH:ubiquinone oxidoreductase (Complex 1) at 22 Å in ice. *J. Mol. Biol.*, **277**, 1033–1046.

Harauz,G. and Ottensmeyer,F.P. (1984) Nucleosome reconstruction via phosphorus mapping. *Science*, **226**, 936–940.

Harauz,G. and Van Heel,M. (1986) Similarity measures between images. Exact filters for general geometry 3D reconstruction. *Optik*, **73**, 146–156.

Heuser,J. (1980) Three-dimensional visualization of coated vesicle formation in fibroblasts. *J. Cell Biol.*, **84**, 560–583.

Heuser,J.E. and Keen,J. (1988) Deep-etch visualization of proteins involved in clathrin assembly. *J. Cell Biol.*, **107**, 877–886.

Heuser,J. and Reese,T.S. (1973) Evidence for recycling of synaptic vesicle membrane during transmitter release at the frog neuromuscular junction. *J. Cell Biol.*, **57**, 315–344.

Kirchhausen,T. and Toyoda,T. (1993) Immunoelectron microscopic evidence for extended conformation of light chains in clathrin trimers. *J. Biol. Chem.*, **268**, 10268–10273.

Kirchhausen,T., Harrison,S.C. and Heuser,J. (1986) Configuration of clathrin trimers: evidence from electron microscopy. *J. Ultrastruct. Mol. Struct. Res.*, **94**, 199–208.

Lemmon,S.K., Pellicena-Palle,A., Conley,K. and Freund,C.L. (1991) Sequence of the clathrin heavy chain from *Saccharomyces cerevisiae* and requirement of the COOH terminal for clathrin function. *J. Cell Biol.*, **112**, 65–80.

Liu,S., Wong,M.L., Craik,C.S. and Brodsky,F.M. (1995) Regulation of clathrin assembly and trimerization defined using recombinant triskelion hubs. *Cell*, **83**, 257–267.

Maycox,P.R., Link,E., Reetz,A., Morris,S.A. and Jahn,R. (1992) Clathrin-coated vesicles in nervous tissue are involved primarily in synaptic vesicle recycling. *J. Cell Biol.*, **6**, 1379–1388.

McLauchlan,H., Newell,J., Morrice,N., Osborne,A., West,M. and Smythe,E. (1997) A novel role for Rab5-GDI in ligand sequestration into clathrin-coated pits. *Curr. Biol.*, **8**, 34–45.

Näthke,I.S., Heuser,J., Lupas,A., Stock,J., Turck,C.W. and Brodsky,F.M. (1992) Folding and trimerization of clathrin subunits at the triskelion hub. *Cell*, **68**, 899–910.

Novick,P. and Zerial,M. (1997) The diversity of Rab proteins in vesicle transport. *Curr. Opin. Cell Biol.*, **9**, 496–504.

Pearse,B.M.F. and Robinson,M.S. (1984) Purification and properties of 100-kd proteins from coated vesicles and their reconstitution with clathrin. *EMBO J.*, **3**, 1951–1957.

Penczek,P., Radermacher,M. and Frank,J. (1992) Three-dimensional reconstruction of single particles embedded in ice. *Ultramicroscopy*, **40**, 33–53.

Penczek,P.A., Grassucci,R.A. and Frank,J. (1994) The ribosome at improved resolution: New techniques for merging and orientation refinement in 3D cryo-electron microscopy of biological particles. *Ultramicroscopy*, **53**, 251–270.

Pishvaee,B., Munn,A. and Payne,G.S. (1997) A novel structural model for regulation of clathrin function. *EMBO J.*, **16**, 2227–2239.

Prior,I.A. and Clague,M.J. (1997) Glutamate uptake occurs at an early stage of synaptic vesicle recycling. *Curr. Biol.*, **7**, 353–356.

Radermacher,M. (1988) Three-dimensional reconstruction from random and nonrandom tilt series. *J. Electron Microsc. Tech.*, **9**, 359–394.

Roth,T.F. and Porter,K.R. (1964) Yolk protein uptake in the oocyte of the mosquito *Aedes aegypti* L. *J. Cell Biol.*, **20**, 313–332.

Schlossman,D.M., Schmid,S.L., Braell,W.A., Rothman,J.E. (1984) An enzyme that removes clathrin coats: purification of an uncoating ATPase. *J. Cell Biol.*, **99**, 723–733.

Schmid,S.L. (1997) Clathrin-coated vesicle formation and protein sorting: an integrated process. *Annu. Rev. Biochem.*, **66**, 511–548.

Solomonia,R.O., McCabe,B.J., Jackson,A.P. and Horn,G. (1997) Clathrin proteins and recognition memory. *Neuroscience*, **80**, 59–67.

Szilágyi,J.F. and Berriman,J. (1994) Herpes simplex virus L particles contain spherical membrane-enclosed inclusion vesicles. *J. Gen. Virol.*, **75**, 1749–1753.

Thon,F. (1966) Zur Defokussierungsabhängigkeit des Phasenkontrastes bei der elektronenmikroskopischen Abbildung. *Z. Naturf.*, **21a**, 476–478.

Toyoshima,C. (1989) On the use of holey grids in electron crystallography. *Ultramicroscopy*, **30**, 439–444.

Ungewickell,E. (1983) Biochemical and immunological studies on clathrin light chains and their binding sites on clathrin triskelions. *EMBO J.*, **2**, 1401–1408.

Ungewickell,E. and Branton,D. (1981) Assembly units of clathrin coats. *Nature*, **289**, 420–422.

Ungewickell,E. and Ungewickell,H. (1991) Bovine brain clathrin light chains impede heavy chain assembly *in vitro*. *J. Cell Biol*., **22**, 12710–12714.

Ungewickell,E., Ungewickell,H., Holstein,S.E.H., Lindner,R., Prasad,K., Barouch,W., Martin,B., Greene,L.E. and Eisenberg,E. (1995) Role of auxilin in uncoating clathrin-coated vesicles. *Nature*, **378**, 632–635.

Van Heel,M. (1987) Similarity measures between images. *Ultramicroscopy*, **21**, 95–99.

Vigers,G.P.A. (1986) Clathrin assemblies in vitreous ice: a structural analysis by image reconstruction. PhD dissertation. University of Cambridge, Cambridge, UK.

Vigers,G.P.A., Crowther,R.A. and Pearse,B.M.F. (1986a) Three-dimensional structure of clathrin cages in ice. *EMBO J*., **5**, 529–534.

Vigers,G.P.A., Crowther,R.A. and Pearse,B.M.F. (1986b) Location of the 100 kd–50 kd accessory proteins in clathrin coats. *EMBO J*., **5**, 2079–2085.

Ybe,J.A., Greene,B., Liu,S.H., Pley,U., Parham,P. and Brodsky,F.M. (1998) Clathrin self-assembly is regulated by three light-chain residues controlling the formation of critical salt bridges. *EMBO J*., **17**, 1297–1303.

Received May 6, 1998; revised and accepted June 29, 1998